Available online at www.sciencedirect.com
SCIENCE DIRECT®
Journal of Computational Physics 202 (2005) 710–736
JOURNAL OF COMPUTATIONAL PHYSICS
www.elsevier.com/locate/jcp

Numerical methods for unsteady compressible multi-component reacting flows on fixed and moving grids

V. Moureau [a,*], G. Lartigue [b], Y. Sommerer [b], C. Angelberger [a], O. Colin [a], T. Poinsot [c]

[a] *Energy Application Techniques Department, IFP, 1 Avenue du Bois Préau, 92500 Rueil-Malmaison, France*
[b] *CERFACS, 42 Avenue G. Coriolis, 31057 Toulouse Cedex, France*
[c] *IMFT, Avenue C. Soula, 31400 Toulouse, France*

Received 12 August 2003; received in revised form 13 July 2004; accepted 2 August 2004
Available online 16 September 2004

Abstract

Deriving high precision schemes to compute turbulent flows on fixed or moving complex grids is becoming a central issue in the direct numerical simulation (DNS) and large eddy simulation (LES) community. The step between classical DNS/LES codes on fixed structured grids and future methods on moving unstructured grids is a significant evolution in terms of numerical methods. For reacting flows, this evolution must also include more precise descriptions of multispecies flows and boundary conditions. This paper describes the development of a method for unsteady multispecies reacting flows on moving grids. The target field of application of this method is DNS and LES but this paper focuses on the method development and elementary test cases. The theoretical basis for the numerical method, the boundary conditions and the moving grid extension are first discussed. Various tests of the method are then provided on fixed and moving grids for simple reacting and non-reacting flows to demonstrate the precision and power of the method in simple reference laminar cases.

Keywords: LES; DNS; ALE; Realistic thermochemistry; High-order methods; Boundary conditions

1. Introduction

The fast development of large eddy simulation (LES) techniques for reacting flows [1,2] is also driving research efforts for specific numerical techniques: this is especially true for gas turbines [3–6] or piston en-

* Corresponding author. Tel.: +33 1 47 52 52 31.
E-mail address: vincent.moureau@centraliens.net (V. Moureau).

0021-9991/$ - see front matter © 2004 Elsevier Inc. All rights reserved.
doi:10.1016/j.jcp.2004.08.003

gines for which LES require non-dissipative schemes able to handle compressible multi-species flows on fixed or moving grids. These schemes must also provide high-order accuracy even though ensuring such a property on arbitrary grids is more difficult than it is on Cartesian grids classically used for DNS for example. Such schemes can not be straightforward extensions of usual Reynolds averaged Navier–Stokes (RANS) solvers in which the levels of numerical viscosity are too high. Maintaining low numerical dissipation in LES computations requires specific efforts in terms of algorithm [7] but also of boundary conditions formulations [1]:

- There is still some controversy about the type of scheme which can be accepted for LES: while upwind schemes [8–11] are sometimes used, most groups try to use spatially centered schemes [12–14] because these schemes are not dissipative. This property is usually considered as necessary to avoid damping small turbulent scales (which are essential in reacting flows) even if these schemes are also more sensitive to oscillations. For 'academic' LES in simple geometries, structured meshes can be used and high-order schemes are easily designed. For complex geometries, however, unstructured methods are mandatory and on such grids, constructing high-order schemes becomes much more difficult. Existing LES solvers for unstructured meshes are limited to second-order [7] or third-order [15] methods. The situation is more complex when such solvers must be used on moving meshes: simple extensions of existing solvers for moving meshes may lead to a loss of the convergence order and an increase of numerical dissipation.
- For compressible reacting flows, specifying boundary conditions becomes critical for LES. The low dissipation of the algorithm required for precision introduces new difficulties: first, errors introduced by approximate boundaries are not damped any more by the scheme (as they were in RANS) so that boundary conditions must generate as few numerical perturbations as possible; second, acoustic waves created by the flow also propagate through the computational domain without damping and must be evacuated through non-reflecting boundaries. Moreover, LES also require to inject turbulence (and sometimes controlled acoustic waves [16]) through inlet boundaries. Methods to reach all these objectives are mostly based on characteristic techniques developed for aerodynamics [1,17–19]. These techniques work for pure gases with constant molecular weights, heat capacities and sound speed. When the gas is a mixture of species, they must be extended to account for variable molecular weights and heat capacities as proposed by Baum et al. [20] for perfect gases or O'Kongo and Bellan [21] for real gases.
- Finally, even the choice of the equations required to describe reacting flows is open to discussion. For a long time, DNS or LES have been restricted to zero heat release flames [22–25] in which fresh and burnt gases had the same temperature: even though this assumption is clearly not satisfied in real flames, such simulations have brought new qualitative information on the physics of turbulent flames. Over the years, multiple other simplifications have appeared in the DNS/LES community: two-dimensional flow [26,27], infinitely fast chemistry, one-step chemistry [27–32], reduced chemistry [33]. Despite the efforts of the DNS/LES community, the precision of the submodels used for DNS or LES is not yet up to what can be done for laminar flames for which precise diffusion models (including the inversion of the diffusion matrix) and complex chemistry can be taken into account: in most existing DNS or LES, the heat capacity C_p of all species is equal and constant while diffusion is usually modeled with Fick's law. These assumptions lead to erroneous flame temperatures (due to the constant C_p approximation) and flame speeds (due to simplification of transport models) which have no real importance in academic problems for turbulent combustion. However, in the last years, the quest for DNS/LES tools has changed: quantitative computations are now required and this leads to difficult choices because it is not possible yet to incorporate all the necessary physics into existing codes. Certain DNS codes now incorporate full chemistry for simple fuels [34–36]: most LES, however, are limited to simpler descriptions. The present study describes a compromise in terms of complexity, precision and cost which has been validated in multiple cases and compared to other codes: the multispecies characteristics of the flow (variable molecular

weights and heat capacities) are fully accounted for, gases are supposed to be perfect, molecular diffusion terms are computed using simplified forms, reduced chemistry schemes can be easily incorporated while preserving the computational parallel efficiency which must remain one of the key features of such codes.

The objectives of this paper are to present the development of a compressible high-order solver for LES of reacting flows on fixed and moving grids. Though the main objective is LES, direct numerical simulations (DNSs) of reacting flows can also be achieved with the same tool. The main features of this solver are summarized below:

- Multi-component compressible reacting gas.
- Unstructured hybrid meshes.
- Explicit time integration.
- Second and third-order spatial accuracy for convective terms on fixed and moving grids.
- Characteristic boundary conditions.

Section 2 first presents the thermochemistry model and the transport equations. The treatment of the boundary conditions in a multi-species gas is presented in Section 3: using different primitive variables leads to a major simplification of the initial formulation of [20]. The integration of the conservation equations on fixed and moving grids is presented in Section 4 for both finite volume and finite element formulations. From this integration, a second-order Lax–Wendroff like scheme is derived in Section 5 and a third-order Taylor–Galerkin scheme is developed in Section 6. Test cases are then described in Section 8: one-dimensional laminar premixed flame on a fixed grid (Section 8.2), uniform flow on a moving grid (Section 8.3), uniformly accelerated piston (Section 8.4) and measurements of convergence order for scalar and vorticity convection (Section 8.5). Finally, conclusions and perspectives of applications are given in Section 9.

2. Thermochemistry model and transport equations

The variables required for the description of a compressible reacting flow are:

$$U = \left(m_x, m_y, m_z, \mathscr{E}, \rho_k\right)^{\mathrm{t}}, \tag{1}$$

where $\vec{m} = (m_x, m_y, m_z)^{\mathrm{t}}$ is the momentum vector, $\mathscr{E}$ is the total non-chemical energy density and ρ_k (for $k = 1$ to N) are the partial densities of the N species present in the mixture. The density ρ is not transported by the solver since it is the sum of the partial densities. The total non-chemical energy is the sum of kinetic energy e_{c} and thermal energy e_{s}:

$$\mathscr{E} = \rho[e_{\mathrm{c}} + e_{\mathrm{s}}] = \rho\left[\frac{1}{2}(u^2 + v^2 + w^2) + \sum_{k=1}^{N} Y_k e_{sk}\right], \tag{2}$$

where Y_k is the mass fraction of species k. The thermal energy e_{sk} of species k is defined by:

$$e_{sk}(T) = \int_0^T C_{vk}(\Theta)\,\mathrm{d}\Theta. \tag{3}$$

To simplify the computation of the energy from temperature (an operation which must be performed at each time step and for each mesh point), the internal energy of each species is tabulated from data bases [37] every 100 K, in a range going from 0 to 5000 K. On each 100 K range, the heat capacity of any species is constant. The energy at a given temperature is then obtained by linear interpolation. This interpolation also provides a fast method to recover temperature from energy data.

The equation of state relating temperature T, pressure P and density ρ is:

$$P = \rho r T. \tag{4}$$

The gas constant of the mixture r is defined from each species gas constant r_k by:

$$r = \sum_{k=1}^{N} Y_k r k = \sum_{k=1}^{N} Y_k \frac{\mathscr{R}}{W_k} = \frac{\mathscr{R}}{W} \quad \text{with} \quad \frac{1}{W} = \sum_{k=1}^{N} \frac{Y_k}{W_k}, \tag{5}$$

where $\mathscr{R} = 8.3143\ \mathrm{J/K/mol}$ is the universal gas constant, W_k is the molar mass of species k and W is the molar mass of the mixture.

The quantities C_p, C_v, r and γ change locally but the usual relations between them still hold:

$$C_\mathrm{p} - C_\mathrm{v} = r \qquad \frac{r}{C_\mathrm{v}} = \gamma - 1 = \beta, \tag{6}$$

where $\gamma = C_\mathrm{p}/C_\mathrm{v}$ is the isentropic coefficient of the mixture.

The equations to solve are the compressible and reacting Navier–Stokes equations, written here in flux-divergence form:

$$\frac{\partial U}{\partial t} + \nabla \cdot \mathscr{F} = \dot{W}, \tag{7}$$

where $\nabla \cdot \mathscr{F}$ is the divergence of the fluxes and $\dot{W}$ is the source terms vector. Each component of the fluxes can be decomposed into three terms: inviscid, viscous and LES contributions.

$$\mathscr{F}_{x,y,z} = \mathscr{F}^{\mathrm{I}}_{x,y,z} + \mathscr{F}^{\mathrm{V}}_{x,y,z} + \mathscr{F}^{\mathrm{LES}}_{x,y,z}. \tag{8}$$

The system of conservative equation (7) can handle both DNS and LES. In the second case the vector U is the vector of *filtered* variables. For simplicity, only DNS cases will be discussed here ($\mathscr{F}^{\mathrm{LES}}_{x,y,z} = 0$), as LES introduces no particular difficulty from the point of view of numerical methods compared to DNS.

The inviscid flux $\mathscr{F}^{\mathrm{I}}$ is defined by:

$$\mathscr{F}^{\mathrm{I}}_x = \begin{pmatrix} \rho u u + P \\ \rho u v \\ \rho u w \\ \rho u E + P u \\ \rho_k u \end{pmatrix}, \quad \mathscr{F}^{\mathrm{I}}_y = \begin{pmatrix} \rho v u \\ \rho v v + P \\ \rho v w \\ \rho v E + P v \\ \rho_k v \end{pmatrix} \quad \text{and} \quad \mathscr{F}^{\mathrm{I}}_z = \begin{pmatrix} \rho w u \\ \rho w v \\ \rho w w + P \\ \rho w E + P w \\ \rho_k w \end{pmatrix}. \tag{9}$$

The viscous fluxes are modeled by:

$$\mathscr{F}^{\mathrm{V}}_i = \begin{pmatrix} -\tau_{ix} \\ -\tau_{iy} \\ -\tau_{iz} \\ -(u\tau_{ix} + v\tau_{iy} + w\tau_{iz}) + q_i \\ \mathscr{J}_{k,i} \end{pmatrix} \tag{10}$$

for $i = x$, y or z. Here, q is the heat flux and $\mathscr{J}_k$ the diffusive flux of the species k. The stress tensor τ is defined by:

$$\tau_{ij} = -\frac{2}{3}\mu \frac{\partial u_k}{\partial x_k}\delta_{ij} + \mu\left(\frac{\partial u_i}{\partial x_j} + \frac{\partial u_j}{\partial x_i}\right), \tag{11}$$

where the molecular viscosity μ is a function of the temperature (through a Sutherland or a power law). This coefficient is defined for the mixture only: there is no influence of the composition on the viscosity.

The diffusive flux of species k is defined by:

$$\mathscr{J}_{k,i} = \rho Y_k V_{k,i}, \tag{12}$$

where $V_{k,i}$ is the ith component of the diffusion velocity of the species k. To ensure mass conservation each component of the flux must verify:

$$\sum_{k=1}^{N} Y_k V_{k,i} = 0. \tag{13}$$

The diffusion velocity $V_{k,i}$ is modeled by the Hirschfelder and Curtis approximation [38]:

$$X_k V_{k,i} = -D_k \frac{\partial X_k}{\partial x_i}, \tag{14}$$

where X_k and D_k are, respectively, the molar fraction and the diffusion coefficient of the species k. This coefficient is computed from the viscosity μ as

$$D_k = \frac{\mu}{\rho Sc_k}, \tag{15}$$

The Schmidt number Sc_k is a constant depending on the species. A major issue [1] is that this formulation does not satisfy (13), i.e. the global mass conservation, if the Schmidt numbers Sc_k are not equal for all species. In this case, a correction velocity V_i^{C} must be added to the diffusion velocity $V_{k,i}$ in (12) to satisfy the continuity equation:

$$\mathscr{J}_{k,i} = \rho Y_k \left(V_{k,i} + V_i^{\mathrm{C}}\right). \tag{16}$$

This correction velocity is defined by:

$$V_i^{\mathrm{C}} = \sum_{j=1}^{N} D_j \frac{W_j}{W} \frac{\partial X_j}{\partial x_i}. \tag{17}$$

The effects of the simplification of the diffusion matrix using the Hirschfelder model and a correction velocity are discussed in [39] or [40]. These effects are very small in most flames using air as oxidizer. The final expression for the species diffusive flux is thus:

$$\mathscr{J}_{k,i} = -\rho D_k \frac{W_k}{W} \frac{\partial X_k}{\partial x_i} + \rho Y_k \left(\sum_{j=1}^{N} D_j \frac{W_j}{W} \frac{\partial X_k}{\partial x_i} \right), \tag{18}$$

which is compatible with total mass conservation.

Finally, the heat flux q is defined by:

$$q_i = -\lambda \frac{\partial T}{\partial x_i} + \sum_{k=1}^{N} \mathscr{J}_{k,i} h_{sk}. \tag{19}$$

The first term is the heat flux due to the classical heat conduction process (Fourier law) while the second term is the heat flux due to the diffusion of species having different enthalpies. The heat conduction coefficient λ is computed from the viscosity μ as:

$$\lambda = \frac{\mu C_{\mathrm{p}}}{Pr}, \tag{20}$$

where the Prandtl number Pr is assumed to be constant: this property is very well satisfied in most air flames.

The source terms vector $\dot{W}$ is defined by:

$$\dot{W} = (0, 0, 0, \dot{\omega}_T, \dot{\omega}_k)^t, \tag{21}$$

where $\dot{\omega}_k$ is the net mass production of the species k due to combustion and $\dot{\omega}_T$ is the associated heat release given by:

$$\dot{\omega}_T = \sum_{k=1}^{N} \Delta h^0_{f,k} \dot{\omega}_k. \tag{22}$$

The standard formation enthalpy $\Delta h^0_{f,k}$ of the species k is also obtained from data bases [37].
The modeling of chemistry is done using classical Arrhenius laws [1,41].

3. Characteristic boundary conditions for multi-component mixtures

Specifying boundary conditions is a critical part in compressible DNS and LES codes [17,19,42]. Characteristic methods are commonly used for compressible aerodynamics codes but require extensions for reacting flows where the gas is a mixture of species for which quantities such as C_p, C_v or r change locally. The method described here is a new formulation of the NSCBC procedure proposed by Poinsot and Lele [43] for mono-component gas and extended by Baum et al. [20] to multi-component mixtures, i.e. a mixture of perfect gases. If the state equation of each gas can not be approximated by a perfect gas law, this formulation can be modified as done for real gases in [21] but the present study does not extend to this case. Note also that, even though the present solver can handle moving grids, the present boundary condition treatment is valid only for fixed boundaries. Imposing boundary conditions on a moving boundary is not necessary in most practical applications (except for the walls of piston engines which can be handled in a simpler way and do not require characteristic treatments).

More generally, the method described here is sufficient for engine computations but would have to be complemented by the use of 'sponge' domains and higher-order wave expansions on the boundaries to handle for example aeroacoustic problems [44–46] which require a higher accuracy on boundaries.

3.1. Extension of the NSCBC method

The NSCBC method proposed in [20] can be ill-posed: there are $5 + N$ variables but one more equation (the relation $\sum Y_k = 1$ or equivalently $\rho = \sum \rho_k$). To avoid this problem, the solution is then either to keep the conservation equation for ρ and to suppress one species equation or to keep all species equations but to suppress the equation for ρ. Here, the choice has been made to keep all species and to leave ρ. The system of equations that is obtained is now perfectly "symmetric" as far as species are concerned.

The second major difference compared to [20] is the choice of primitive variables. The primitive variable associated to energy is not temperature but pressure. For the species, the partial densities ρ_k are taken as primitive variables instead of mass fractions Y_k. This simplifies drastically the formulation.

3.2. Recasting equations from conservative to primitive variables

The Navier–Stokes equation (7) have previously been written in terms of flux of conservative variables. This form is very well suited for the discretization in the finite volume context. However, for deriving boundary conditions, it is easier to rewrite the equations in the quasi-linear primitive form. Moreover, the velocity components are written in a generic direct orthonormal basis $(\vec{n}, \vec{t}_1, \vec{t}_2)$, in which $\vec{u} = (u_n, u_{t1}, u_{t2})^t$. The $\vec{n}$ direction corresponds to the outgoing normal vector on boundaries. Characteristic analysis [17,18] leads to a new form of the conservation equations:

$$\frac{\partial V}{\partial t} + d = T, \tag{23}$$

where $V = (u_n, u_{t1}, u_{t2}, P, \rho_1, \ldots, \rho_N)^t$ is the primitive variable vector. The d term (also called normal term) represents the contributions of the derivatives along $\vec{n}$:

$$\begin{pmatrix} d_{u_n} \\ d_{u_{t1}} \\ d_{u_{t2}} \\ d_P \\ d_{\rho_k} \end{pmatrix} = \begin{pmatrix} u_n \frac{\partial u_n}{\partial \vec{n}} + \frac{1}{\rho}\frac{\partial P}{\partial \vec{n}} \\ u_n \frac{\partial u_{t1}}{\partial \vec{n}} \\ u_n \frac{\partial u_{t2}}{\partial \vec{n}} \\ u_n \frac{\partial P}{\partial \vec{n}} + \rho c^2 \frac{\partial u_n}{\partial \vec{n}} \\ u_n \frac{\partial \rho_k}{\partial \vec{n}} + \rho_k \frac{\partial u_n}{\partial \vec{n}} \end{pmatrix}, \tag{24}$$

where $\frac{\partial \alpha}{\partial \vec{n}} = \frac{\partial \alpha}{\partial x} n_x + \frac{\partial \alpha}{\partial y} n_y + \frac{\partial \alpha}{\partial z} n_z$.

This can be written in matrix notation:

$$d = E_{\vec{n}} \cdot \frac{\partial V}{\partial \vec{n}}, \tag{25}$$

where $E_{\vec{n}}$ is the Jacobian matrix of the system:

$$E_{\vec{n}} = \begin{pmatrix} u_n & 0 & 0 & \frac{1}{\rho} & 0 & \ldots & 0 \\ 0 & u_n & 0 & 0 & 0 & \ldots & 0 \\ 0 & 0 & u_n & 0 & 0 & \ldots & 0 \\ \rho c^2 & 0 & 0 & u_n & 0 & \ldots & 0 \\ \rho_1 & 0 & 0 & 0 & u_n & \ldots & 0 \\ \vdots & \vdots & \vdots & \vdots & \vdots & \ddots & \vdots \\ \rho_N & 0 & 0 & 0 & 0 & \ldots & u_n \end{pmatrix}. \tag{26}$$

The T term represents all the other contributions (tangential, diffusion, reaction).

3.3. The characteristic variables

The matrix $E_{\vec{n}}$ can be diagonalized and this decomposition allows to write convection equations for the waves amplitudes:

$$\frac{\partial A}{\partial t} + \lambda \frac{\partial A}{\partial \vec{n}} = T_A, \tag{27}$$

where A is the wave amplitude, λ is the wave convection velocity and T_A is the sum of all non-hyperbolic terms associated to the wave.

The amplitudes of the $4 + N$ waves can be written as

$$\begin{pmatrix} \partial A_+ \\ \partial A_- \\ \partial A_{t1} \\ \partial A_{t2} \\ \partial A_k \end{pmatrix} = \begin{pmatrix} \partial u_n + \frac{1}{\rho c}\partial P \\ \partial u_n - \frac{1}{\rho c}\partial P \\ \partial u_{t1} \\ \partial u_{t2} \\ -\frac{Y_k}{c^2}\partial P + \partial \rho_k \end{pmatrix} \tag{28}$$

and the associated convection velocities are:

$$\begin{pmatrix} \lambda_+ \\ \lambda_- \\ \lambda_{t1} \\ \lambda_{t2} \\ \lambda_k \end{pmatrix} = \begin{pmatrix} u_n + c \\ u_n - c \\ u_n \\ u_n \\ u_n \end{pmatrix}. \tag{29}$$

Keeping the notation $\mathscr{L} = \lambda \frac{\partial A}{\partial \vec{n}}$ of [43] for the waves amplitude variations, the normal term d of (24) is:

$$\begin{pmatrix} d_{u_n} \\ d_{u_{t1}} \\ d_{u_{t2}} \\ d_P \\ d_{\rho_k} \end{pmatrix} = \begin{pmatrix} \frac{1}{2}(\mathscr{L}_+ - \mathscr{L}_-) \\ \mathscr{L}_{t1} \\ \mathscr{L}_{t2} \\ \frac{\rho c}{2}(\mathscr{L}_+ + \mathscr{L}_-) \\ \frac{\rho_k}{2c}(\mathscr{L}_+ + \mathscr{L}_-) + \mathscr{L}_k \end{pmatrix}. \tag{30}$$

The acoustic waves $\mathscr{L}_+$ and $\mathscr{L}_-$ are convected, respectively, at the velocity $u_n + c$ and $u_n - c$. All other waves are convected with the flow at the velocity u_n. The waves $\mathscr{L}_{t1}$ and $\mathscr{L}_{t2}$ are known as shear waves. The remaining waves $\mathscr{L}_k$ (for $k = 1$ to N) are species waves. No wave can easily be identified with the classical entropy wave because density is not directly solved for. However, all species waves $\mathscr{L}_k$ have the same convection velocity u_n and any linear combination of these waves is still a wave convected at the velocity u_n. For example

$$\mathscr{L}_S = \sum_{k=1}^{N} \mathscr{L}_k = u_n \left(-\frac{1}{c^2} \frac{\partial P}{\partial \vec{n}} + \frac{\partial \rho}{\partial \vec{n}} \right) \tag{31}$$

is proportional to the entropy wave given by Poinsot and Lele [43].

3.4. The LODI relations

The central idea of characteristic methods for boundary conditions is to identify the outgoing and incoming waves crossing a boundary. The outgoing waves carry information from the interior of the domain and must be kept as computed by the numerical scheme. However, the incoming waves carry information coming from the outside (i.e. controlled by the boundary condition). They cannot be computed from interior points data. The principle of the present method is to infer the amplitude of the incoming waves from the amplitude of the outgoing waves and from some appropriate LODI (local one-dimensional inviscid) relations [43]. These LODI relations are obtained by writing (23) near the boundary as if the flow was locally inviscid and one-dimensional. Of course, at this point, the physical behaviour of the boundary must be taken into account to choose which LODI relation should be used. Some examples of LODI relations are given below:

$$\frac{\partial P}{\partial t} + \frac{\rho c}{2}(\mathscr{L}_+ + \mathscr{L}_-) = 0, \tag{32}$$

$$\frac{\partial u_n}{\partial t} + \frac{1}{2}(\mathscr{L}_+ - \mathscr{L}_-) = 0, \tag{33}$$

$$\frac{\partial u_{t1}}{\partial t} + \mathscr{L}_{t1} = 0, \tag{34}$$

$$\frac{\partial u_{t2}}{\partial t} + \mathscr{L}_{t2} = 0, \tag{35}$$

$$\frac{\partial \rho_k}{\partial t} + \frac{\rho_k}{2c}(\mathscr{L}_+ + \mathscr{L}_-) + \mathscr{L}_k = 0, \tag{36}$$

$$\frac{\partial \rho}{\partial t} + \frac{\rho}{2c}(\mathscr{L}_+ + \mathscr{L}_-) + \mathscr{L}_S = 0, \tag{37}$$

$$\frac{\partial Y_k}{\partial t} + \frac{1}{\rho}(\mathscr{L}_k - Y_k \mathscr{L}_S) = 0, \tag{38}$$

$$\frac{\partial r}{\partial t} + \frac{1}{\rho}(r\mathscr{L}_S + \sum r_k \mathscr{L}_k) = 0, \tag{39}$$

$$\frac{\partial T}{\partial t} + \frac{\beta T}{2c}(\mathscr{L}_+ + \mathscr{L}_-) - \frac{T}{\rho r}\sum r_k \mathscr{L}_k = 0. \tag{40}$$

Additional LODI equations can be written for enthalpy, entropy, momentum or for normal gradients.

3.5. Example of practical implementation

From the LODI relations, it is straightforward to write various characteristic boundary conditions using the technique described in [43]. Only a single example is given here: a subsonic inlet with time-varying velocity, temperature and composition. For a subsonic inlet, only the backward travelling acoustic wave $\mathscr{L}_-$ is leaving the computational domain while the $3 + N$ other waves are entering it. Since $\mathscr{L}_-$ leaves the domain it can be evaluated using (28) and one-sided derivatives. To determine the $3 + N$ incoming waves $\mathscr{L}_+$, $\mathscr{L}_{t1}$ and $\mathscr{L}_{t2}$, the nature of the boundary suggests to use the LODI relations (33)–(35).

$$\mathscr{L}_+ = \mathscr{L}_- - 2\frac{\partial u_n^{\mathrm{t}}}{\partial t}, \tag{41}$$

$$\mathscr{L}_{t1} = -\frac{\partial u_{t1}^{\mathrm{t}}}{\partial t}, \tag{42}$$

$$\mathscr{L}_{t2} = -\frac{\partial u_{t2}^{\mathrm{t}}}{\partial t}. \tag{43}$$

The 't' superscript is here to remind that the values in the temporal derivatives are the "target" values to impose on the boundary (for example, a turbulent or an acoustic signal). To find the N remaining $\mathscr{L}_k$ waves, (40) is used to have:

$$\sum_{k=1}^{N} r_k \mathscr{L}_k = \frac{\rho r}{T}\left(\frac{\partial T^{\mathrm{t}}}{\partial t} + \frac{\beta T}{c}\left(\mathscr{L}_- - \frac{\partial u_n^{\mathrm{t}}}{\partial t}\right)\right). \tag{44}$$

Introducing this value in (39) gives for the entropy wave:

$$\mathscr{L}_S = -\frac{\rho}{T}\frac{\partial T^{\mathrm{t}}}{\partial t} - \rho\sum_{k=1}^{N}\frac{r_k}{r}\frac{\partial Y_k^{\mathrm{t}}}{\partial t} + \frac{\rho\beta}{c}\left(\frac{\partial u_n^{\mathrm{t}}}{\partial t} - \mathscr{L}_-\right) \tag{45}$$

and finally, using (38), the species waves are:

$$\mathscr{L}_k = Y_k \mathscr{L}_S - \rho\frac{\partial Y_k^{\mathrm{t}}}{\partial t}. \tag{46}$$

The 3 + N waves $\mathscr{L}_+$, $\mathscr{L}_{t1}$, $\mathscr{L}_{t2}$ and $\mathscr{L}_k$ are now specified. These values and the scheme-computed value of $\mathscr{L}_-$ can then be put back in the normal terms vector d and the variables on the boundary can be updated for the next time-step using (23). An additional difficulty associated to the use of characteristic boundary conditions is the possible drift of mean values. This drift can be controlled in the present approach by adding corrective terms in (41)–(43) and (46). This corrective treatment follows the methods proposed in [1,42,43].

4. Integration of the conservation equations on dynamic meshes

Solving the Navier–Stokes equations on a deforming domain $\Omega(t)$ is usually achieved using a body-force method [47] or an arbitrary Lagrangian–Eulerian (ALE) method [48]. The body-force method consists of imposing a given speed on an arbitrary surface which does not necessarily coincide with the mesh. Complex deforming geometries can be simulated on fixed Cartesian grids with this method but an important drawback is that imposing characteristic boundary conditions as described in the previous section is very difficult. An appealing alternative is the ALE method in which each mesh node i has a given displacement speed $\dot{X}_i(t)$ and the boundaries of the computational domain $\partial\Omega(t)$ coincide with mesh vertices. In conjunction with the ALE approach, the characteristic method developed in Section 3 can be used for inlets and outlets, which are fixed in most simulations of real applications (gas turbines, piston engines). The moving parts (blades, pistons) are generally rigid walls and can therefore be considered as being perfectly reflective. This kind of acoustic boundary condition can be easily achieved by imposing directly the velocity. For this reason, no specific acoustic boundary condition for moving walls was developed.

This section presents the formalism used to integrate the Navier–Stokes equations on moving grids for finite volume (FV) and finite element (FE) methods. The originality of the following approach is the generalization of existing fixed-grid schemes to moving grids. In the case of fluid–structure interactions or free-surface flows, the grid velocities and the mesh deformations may reach high values and specific numerical schemes must be designed. For example, Masud et al. [49] and Tezduyar et al. [50] have described finite-element schemes adapted for such flows. Concerning gas turbines and piston engines, the position and the velocity of the boundaries are always known and the grid velocities and the mesh deformations are much lower. In this case, fixed-grid numerical schemes are useable provided that they have been modified to handle moving meshes. This can be done by introducing a time dependency of the volumes and of the test functions. If this generalization is rigorously done, the resulting schemes should have the same numerical properties than their fixed-grid equivalents.

Considering the Navier–Stokes equations written in the partial derivative form:

$$\frac{\partial U}{\partial t} + \nabla \cdot (\mathscr{F}^{\mathrm{I}} + \mathscr{F}^{\mathrm{V}}) = \dot{W} \tag{47}$$

the source terms $\dot{W}$ do not involve spatial gradients and their implementation in an explicit code is straightforward. These terms are therefore left out of the remainder of the derivation. Due to the different nature of the inviscid fluxes $\mathscr{F}^{\mathrm{I}}$ and viscous fluxes $\mathscr{F}^{\mathrm{V}}$, two different types of numerical schemes must be applied on each. The diffusion fluxes $\mathscr{F}^{\mathrm{V}}$ do not raise specific difficulties and are treated here with a standard second-order centered scheme. The critical term for LES and DNS is the inviscid flux $\mathscr{F}^{\mathrm{I}}$ and the numerical schemes presented here only apply to this inviscid part. From now on, the inviscid fluxes $\mathscr{F}^{\mathrm{I}}$ are simply written $\mathscr{F}$. The conservative variables U and the fluxes $\mathscr{F}$ are considered to be functions of the grid position and time: $U(X,t)$ and $\mathscr{F}(X,t)$. To simplify the derivation of the schemes, the grid velocity $\dot{X}_i(t)$ is supposed constant during a computational time step Δt. Since the time steps are small compared to the simulation time, it does not limit the generality of the method.

4.1. Finite volume schemes

The spatial integration for FV schemes is developed for arbitrarily node-centered control volumes V_i. The integration of (47) with Leibniz transport theorem gives:

$$\int_{t^n}^{t^{n+1}} \frac{\mathrm{d}}{\mathrm{d}t} \int_{V_i(t)} U \,\mathrm{d}V \,\mathrm{d}t + \int_{t^n}^{t^{n+1}} \int_{V_i(t)} \nabla \cdot (\mathscr{F} - \dot{X}U) \,\mathrm{d}V \,\mathrm{d}t = 0. \tag{48}$$

Referring to the second term of the left-hand side of (48) as $\Delta t V_i^{n+\frac{1}{2}} R_i$ and using the FV approximation for the first term gives:

$$V_i^{n+1} U_i^{n+1} - V_i^n U_i^n = -\Delta t V_i^{n+\frac{1}{2}} R_i. \tag{49}$$

Eq. (49) is a generic form for ALE one-step FV schemes where the expression of the residual R_i determines the scheme type. The use of the volume $V_i^{n+\frac{1}{2}}$ is justified in Section 5.

4.2. Finite element schemes

After choosing suitable scalar test functions ϕ_i for $1 \leqslant i \leqslant N_p$, where N_p is the number of mesh points, and applying the Galerkin method, (47) becomes:

$$\int_{t^n}^{t^{n+1}} \int_{\Omega(t)} \phi_i \frac{\partial U}{\partial t} U \,\mathrm{d}V \,\mathrm{d}t + \int_{t^n}^{t^{n+1}} \int_{\Omega(t)} \phi_i \nabla \cdot \mathscr{F} \,\mathrm{d}V \,\mathrm{d}t = 0. \tag{50}$$

The scalar test functions depend only on the node position. Thus they satisfy a conservation relation:

$$\frac{\mathrm{D}\phi_i}{\mathrm{D}t} \phi_i = 0 \quad \text{where} \quad \frac{\mathrm{D}}{\mathrm{D}t} = \frac{\partial U}{\partial t} + \dot{X} \cdot \nabla. \tag{51}$$

Eq. (51) and Leibniz transport theorem leads to:

$$\int_{t^n}^{t^{n+1}} \frac{\mathrm{d}}{\mathrm{d}t} \int_{\Omega(t)} \phi_i U \,\mathrm{d}V \,\mathrm{d}t + \int_{t^n}^{t^{n+1}} \int_{\Omega(t)} \phi_i \nabla \cdot (\mathscr{F} - \dot{X}U) \,\mathrm{d}V \,\mathrm{d}t = 0. \tag{52}$$

Then U is decomposed on the scalar test functions base as follows:

$$U(X) = \sum_{k=1}^{N_p} \phi_k(X) U_k. \tag{53}$$

Defining the mass matrix:

$$M_{ik} = \int_{\Omega} \phi_i \phi_k \,\mathrm{d}V \tag{54}$$

and the FE residual S:

$$\Delta t S = \int_{t^n}^{t^{n+1}} \int_{\Omega(t)} \phi_i \nabla \cdot (\mathscr{F} - \dot{X}U) \,\mathrm{d}V \,\mathrm{d}t \tag{55}$$

the generic form for ALE one-step FE schemes is:

$$\sum_{k=1}^{N_p} M_{ik}^{n+1} U_k^{n+1} - \sum_{k=1}^{N_p} M_{ik}^n U_k^n = -\Delta t S. \tag{56}$$

The exact formulation of S determines the scheme type.

5. Formulation of the FV Lax–Wendroff scheme on dynamic meshes

The Lax–Wendroff scheme is the simplest second-order centered finite volume scheme. On fixed grids, it is obtained by performing a time centered second-order Taylor development of U and replacing the temporal derivatives with spatial derivatives. For dynamic meshes, the Taylor developments must be done after the spatial integration in order to take into account the mesh movement.

5.1. Derivation

The residual R_i of (49) is written as

$$\Delta t V_i^{n+\frac{1}{2}} R_i = \int_{t^n}^{t^{n+1}} Q_i(t)\,\mathrm{d}t, \tag{57}$$

where

$$Q_i(t) = \int_{V_i(t)} \nabla\cdot(\mathscr{F} - \dot{X}U)\,\mathrm{d}V. \tag{58}$$

As the scheme is centered, $Q_i(t)$ is developed at the second order in time around $t^{n+\frac{1}{2}}$:

$$Q_i(t) = Q_i^{n+\frac{1}{2}} + (t - t^{n+\frac{1}{2}})\frac{\mathrm{d}Q_i}{\mathrm{d}t} + \mathrm{O}[(t - t^{n+\frac{1}{2}})^2]. \tag{59}$$

Consequently, the residual is expressed as follows:

$$\Delta t V_i^{n+\frac{1}{2}} R_i = \Delta t Q_i(t^{n+\frac{1}{2}}) + \mathrm{O}[\Delta t^3] \approx \Delta t \int_{V_i^{n+\frac{1}{2}}} \nabla\cdot(\mathscr{F}^{n+\frac{1}{2}} - \dot{X}U^{n+\frac{1}{2}})\,\mathrm{d}V. \tag{60}$$

For the scheme to remain explicit, fluxes and conservative variables of Eq. (60) must be expanded in time as:

$$U^{n+\frac{1}{2}} = U^n + \frac{\Delta t}{2}\left.\frac{\partial U}{\partial t}\right|_{t^n} + \frac{\Delta t}{2}(\dot{X}\cdot\vec{\nabla})U^n, \tag{61}$$

$$\mathscr{F}^{n+\frac{1}{2}} = \mathscr{F}^n + \frac{\Delta t}{2}\left.\frac{\partial \mathscr{F}}{\partial t}\right|_{t^n} + \frac{\Delta t}{2}(\dot{X}\cdot\vec{\nabla})\mathscr{F}^n. \tag{62}$$

Introducing the flux Jacobian A and using (47), the final formulation of the residual is obtained:

$$R_i = \frac{1}{V_i^{n+\frac{1}{2}}}\int_{V_i^{n+\frac{1}{2}}} \nabla\cdot(\mathscr{F}^n - \dot{X}U^n)\,\mathrm{d}V - \frac{\Delta t}{2V_i^{n+\frac{1}{2}}}\int_{V_i^{n+\frac{1}{2}}} \nabla\cdot[A^n - I\dot{X}] \times \left(\nabla\cdot(\mathscr{F}^n - \dot{X}U^n) + U^n(\nabla\cdot\dot{X})\right)\mathrm{d}V. \tag{63}$$

Eq. (63) corresponds to the time integrated formulation of the FV Lax–Wendroff schemes. To obtain the discrete formulation, the spatial integrations have to be replaced by suitable FV approximations.

5.2. Interpretation

The ALE formulation of the Lax–Wendroff scheme (63) differs from the classical scheme on two main points. The first concerns the integration volumes which are taken at the middle of the time step. Recalling that Lax–Wendroff is a centered scheme justifies the use of these volumes. The second point is the emergence of correcting terms of two types:

- $-\dot{X}U^n$ for the fluxes and $-I\dot{X}$ for the Jacobian,
- volumes in $V_i^{n+1}U_i^{n+1} - V_i^nU_i^n$ in (49) and $U^n(\nabla\cdot\dot{X})$ in the second order operator of (63).

The first terms take into account the movement of the nodes. The second terms come from the mesh dilatation. The term $\nabla\cdot\dot{X}$ appears indeed in the geometrical relation:

$$V_i^{n+1} - V_i^n = \Delta t\int_{V_i^{n+\frac{1}{2}}}(\nabla\cdot\dot{X})\,\mathrm{d}V. \tag{64}$$

The correcting terms ($-I\dot{X}$ and $U^n(\nabla\cdot\dot{X})$) in the second-order operator of (63) are non-intuitive terms required to maintain the accuracy of the method.

6. Formulation of the TTGC scheme on dynamic meshes

TTGC is a two-step Taylor–Galerkin FE scheme developed by Colin and Rudgyard [15] that provides a third-order spatial and temporal accuracy. It has been specifically written for LES applications by minimizing the numerical dissipation of the small scales. On fixed grids this scheme is written under partial derivative form:

$$\tilde{U}^n = U^n + \alpha\Delta t\frac{\partial U}{\partial t} + \beta\Delta t^2\frac{\partial^2 U}{\partial t^2}, \tag{65}$$

$$U^{n+1} = U^n + \Delta t\frac{\partial \tilde{U}}{\partial t} + \gamma\Delta t^2\frac{\partial^2 U}{\partial t^2}. \tag{66}$$

On fixed grids, the Galerkin method is applied to these equations and suitable approximations are made to obtain the discrete spatial operators. However, for dynamic meshes the Galerkin method cannot be directly applied to (65) and (66). Consequently, the derivation starts from (49) where the Galerkin method has already been applied and the mesh movement has been taken into account. The discretization is done as if the two steps were two time steps of duration $\alpha\Delta t$ ($0<\alpha<0.5$) and Δt, respectively. Then the same methodology as the Lax–Wendroff scheme is used. The Taylor developments are done in the time integral introducing the Jacobian and paying attention to the development coefficients. Finally, the scheme takes the time integrated form:

$$\tilde{M}^{n+\alpha}\tilde{U} - M^nU^n = -\Delta t\left[\alpha L^{n+\frac{\alpha}{2}}(U^n) + \Delta t\beta LL^{n+\frac{\alpha}{2}}(U^n)\right], \tag{67}$$

$$M^{n+1}U^{n+1} - M^nU^n = -\Delta t\left[L^{n+\frac{1}{2}}(\tilde{U}^n) + \Delta t\gamma LL^{n+\frac{1}{2}}(U^n)\right], \tag{68}$$

where

$$L^{n+\frac{\alpha}{2}}(U^n) = \int_{\Omega^{n+\frac{\alpha}{2}}}\phi_i\nabla\cdot(\mathscr{F}^n - \dot{X}U^n)\,\mathrm{d}V, \tag{69}$$

$$LL^{n+\frac{\alpha}{2}}(U^n) = \int_{\Omega^{n+\frac{\alpha}{2}}}\phi_i\nabla\cdot[A^n - I\dot{X}]\left(\nabla\cdot(\mathscr{F}^n - \dot{X}U^n) + U^n(\nabla\cdot\dot{X})\right)\mathrm{d}V. \tag{70}$$

When writing $\dot{X}=0$ in (69) and (70), the fixed grid method is recovered. Compared to the Lax–Wendroff scheme on moving grids the same correcting terms appear except $V_i^{n+1}U_i^{n+1} - V_i^nU_i^n$ which becomes $M^{n+1}U^{n+1} - M^nU^n$.

7. Geometric conservation properties of the schemes

The integration of the Navier–Stokes equations on fixed meshes requires special care to ensure the exact conservation of quantities as mass or momentum. On dynamic grids, extra geometric properties must also be satisfied to conserve the surfaces and the volumes during the computation. Farhat [51] has shown that satisfying this set of properties called the geometric conservation law (GCL) is a necessary condition for first-order time accuracy. Schemes which do not verify this law, generate non-physical perturbations.

As the numerical scheme, the GCL can be written under many forms: partial derivative form (or continuous), time integrated form, time and space integrated form (or discrete form). Each form of the GCL (CGCL, TIGCL and DGCL) is associated to a different level of discretization. The most important form is the discrete one (DGCL) which is involved in the numerical solver. Moreover these forms are different depending on the formalism (FV or FE).

This section demonstrates that the numerical schemes developed on dynamic meshes in the previous sections satisfy the different forms of the GCL.

7.1. FV forms of the GCL

For every mobile volume in the computational domain the FV continuous GCL (CGCL) is written as

$$\frac{\mathrm{d}}{\mathrm{d}t}\int_{V(t)}\mathrm{d}V=\int_{\partial V(t)}\dot{X}\cdot\vec{dS}=\int_{V(t)}\nabla\cdot\dot{X}\,\mathrm{d}V. \tag{71}$$

After time-integration, (71) becomes:

$$V^{n+1}-V^{n}=\int_{t^n}^{t^{n+1}}\int_{\partial V(t)}\dot{X}\cdot\vec{dS}\,\mathrm{d}t. \tag{72}$$

Following the main hypothesis that $\dot{X}$ is constant during a time step, the surface vectors $\vec{dS}$ vary linearly in time. Consequently, (72) is equivalent to the time integrated GCL (TIGCL):

$$V^{n+1}-V^{n}=\Delta t\int_{\partial V^{n+\frac{1}{2}}}\dot{X}\cdot\vec{dS}=\Delta t\int_{V^{n+\frac{1}{2}}}\nabla\cdot\dot{X}\,\mathrm{d}V. \tag{73}$$

Replacing the spatial integrals of (73) by exact discrete summations leads to the discrete form of the GCL (DGCL).

Showing that the Lax–Wendroff scheme developed in Section 5 satisfies the GCL is done by considering a uniform flow $U(X,t) = U_0$. In this case (48) leads directly to the CGCL and (49) and (63) lead to the TIGCL. The verification of the DGCL is subordinated to the discretization of the spatial operators of the scheme.

7.2. FE forms of the GCL

For FE schemes the CGCL takes the form:

$$\frac{\mathrm{d}}{\mathrm{d}t}\int_{\Omega(t)}\phi_i\,\mathrm{d}V=\int_{\Omega(t)}\phi_i\nabla\cdot\dot{X}\,\mathrm{d}V. \tag{74}$$

During a time step the test functions and the grid velocity only depend on the mesh position implying:

$$\frac{\mathrm{D}}{\mathrm{D}t}\left(\phi_i\nabla\cdot\dot{X}\right)=0. \tag{75}$$

This relation is used to replace the right-hand term of (74) and obtain the FE TIGCL:

$$\int_{\Omega^{n+1}} \phi_i \, \mathrm{d}V - \int_{\Omega^n} \phi_i \, \mathrm{d}V = \Delta t \int_{\Omega^{n+\frac{1}{2}}} \phi_i \nabla \cdot \dot{X} \, \mathrm{d}V. \tag{76}$$

The same methodology as for the Lax–Wendroff scheme is used. When the flow is uniform:

$$U_i = \omega_0 = ((\rho u)_0, (\rho v)_0, (\rho w)_0, (\rho E)_0, (\rho Y_k)_0)^{\mathrm{t}} \quad \text{for each node } i. \tag{77}$$

Eq. (50) leads to the FE form of the CGCL. For the TIGCL, the mass matrix multiplied by U gives:

$$(MU)_k = \left(\omega_0 \sum_{i=1}^{N_p} \int_{\Omega} \phi_i \phi_k \, \mathrm{d}\Omega \right)_k = \left(\omega_0 \int_{\Omega} \phi_k \, \mathrm{d}\Omega \right)_k. \tag{78}$$

Therefore, Eqs. (78) and (67) to (70) lead to (76). It means that the TTGC scheme on dynamic meshes satisfies the TIGCL. The verification of the DGCL depends on the discretization of the spatial operators in Eq. (69) and (70).

8. Validation test cases

8.1. Note on the solver used for the validation test cases

All the previous developments have been implemented in an existing solver: the AVBP code (jointly developed by IFP and CERFACS). Results presented below have all been obtained with this solver.

8.2. One-dimensional flame

The aim of this test is to check the accuracy of both the thermochemistry model and the boundary conditions on a fixed grid. A one-dimensional methane/air flame with 6 species and 2 reactions is simulated (see [52] for more details about this scheme):

$$\mathrm{CH_4} + \frac{3}{2}\mathrm{O_2} \rightarrow \mathrm{CO} + 2\mathrm{H_2O} \tag{79}$$

$$\mathrm{CO} + \frac{1}{2}\mathrm{O_2} \rightleftharpoons \mathrm{CO_2} \tag{80}$$

The inlet and the outlet are non-reflecting. The main parameters of this computation are given in Table 1. After a transient time following the initialization where acoustic waves are evacuated by the boundary conditions, the computation converges and the steady solution is plotted in Figs. 1 and 2. A solution obtained with the PREMIX tool from the CHEMKINpackage is also given as a reference. The PREMIX solver is the reference code for the simulation of one-dimensional laminar flames with complex transport and chemistry. Figs. 1 and 2 show that the temperature and species mass fractions profiles predicted by AVBP and PREMIX are very close. The maximum flame temperatures are nearly the same for AVBP (2260 K) and PREMIX (2252 K).

The flame speeds predicted by AVBP (38.06 cm/s) and PREMIX (36.66 cm/s also match very well, confirming that the level of precision used for thermodynamic and chemical data is sufficient. The small differences between the two codes may be explained by the numerical method, the thermodynamic databases and the computation of the diffusion coefficients that are treated differently in the two codes. Finally, the time evolutions of inlet and outlet pressure are presented in Fig. 3 to show the non-reflecting character of the boundary conditions: a first wave due to the initialization reaches both outlet and inlet at $t = 2$ ms, it leaves the

Table 1
Computation parameters

Equivalence ratio	Fresh gases temperature	Pressure	Mesh size
1.00	300 K	101,300 Pa	$\Delta x = 50$ μm

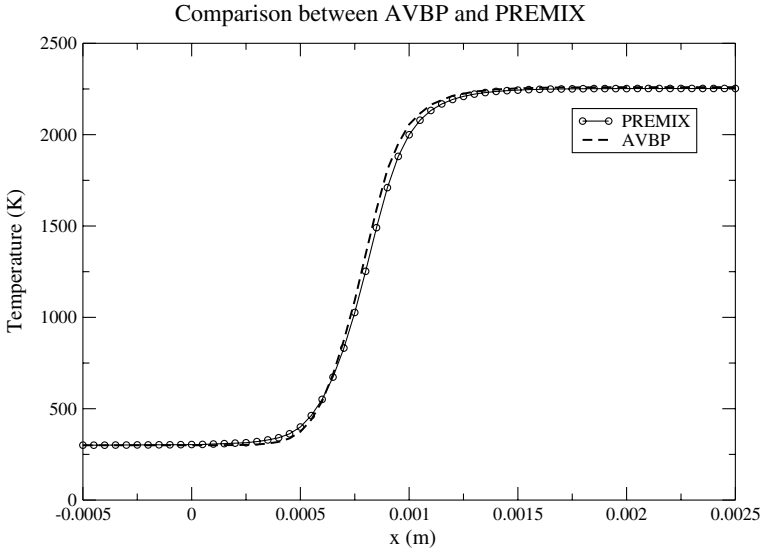

Fig. 1. Flame temperature profile.

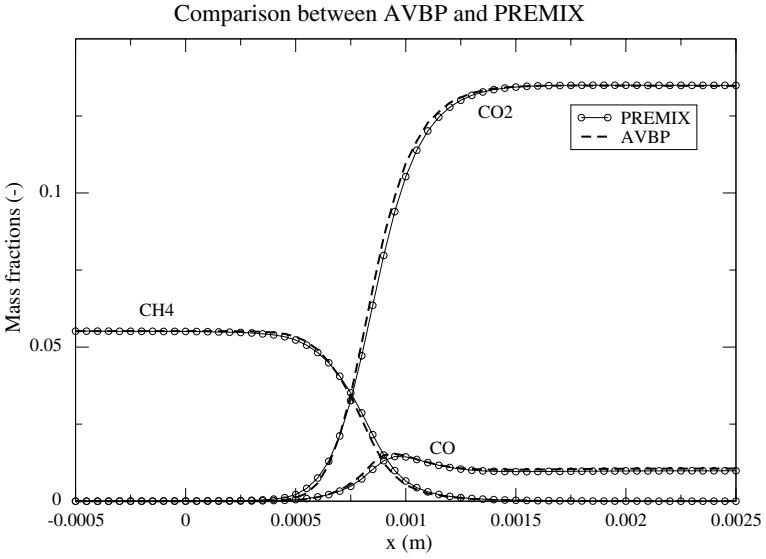

Fig. 2. Flame mass fractions profile.

domain through the boundaries and no reflection takes place. After 5 ms, the acoustic activity at both ends of the domain is zero and both pressures are constant.

8.3. Uniform flow

Simulating this case allows to check if a numerical scheme really satisfies the discrete form of the GCL. It consists of a closed box with a uniform mixture initially at rest. The boundaries of the box are fixed but the mesh points are moving. The initial meshes used in this case are an unstructured triangular grid (TRI) and a regular quadrangular grid (QUAD). The deformation law of the mesh is a periodic radial contraction-expansion distortion illustrated in Fig. 4. The simulation time corresponds to hundred periods τ_D of the deformation law. For schemes that satisfy the discrete GCL the flow should remain uniformly at rest. An estimation of the numerical error is thus defined by:

$$\text{error} = \frac{K}{\frac{1}{\tau_D}\int_{\tau_D}\left\langle \frac{1}{2}|\dot{X}|^2 \right\rangle \mathrm{d}t}, \tag{81}$$

which is the ratio of the mean kinetic energy K of the flow and a mean grid kinetic energy averaged in time. Fig. 5 shows this error for different schemes and meshes: if it remains equal to zero the DGCL criterion is satisfied. The tests performed confirm the theoretical analysis from the previous section: the DGCL is satisfied for all combinations, except for TTGC on irregular bilinear elements. However even in this case, the error is small, leading only to negligible perturbations.

8.4. Uniformly Accelerated Piston

A uniformly accelerated piston (UAP) induces an acoustic wave (see Fig. 6) for which analytical solutions have been given by Landau and Lifchitz [53]. The simulation time is limited by the reflection of the wave on the opposite wall to the piston and by the piston speed which must remain small compared

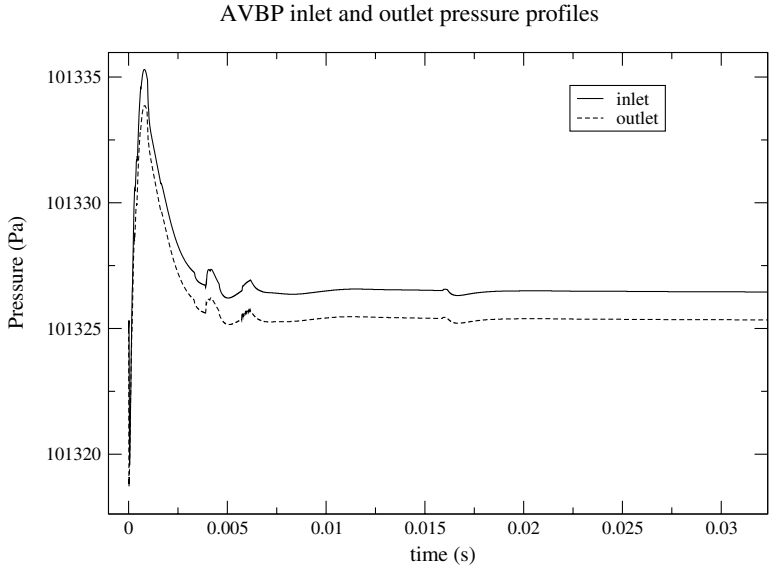

Fig. 3. Time evolution of inlet and outlet pressure for flame computation.

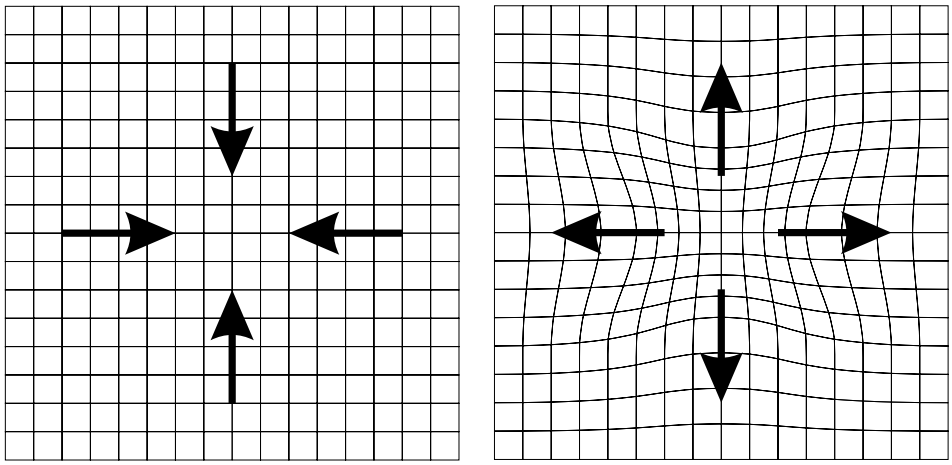

Fig. 4. Mesh deformations.

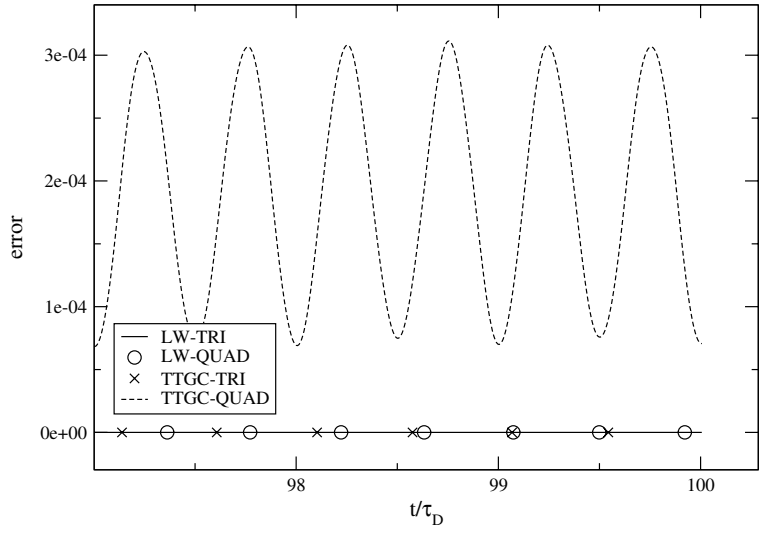

Fig. 5. Kinetic energy error.

to the speed of sound in order to avoid creating a shock. The Lax–Wendroff and TTGC schemes are tested on two meshes composed of regular triangles (TRI) or regular quadrangles (QUAD), respectively. The elements remain regular with time as the meshes are uniformly distorted. For each scheme, five velocity profiles at different times are compared to the analytical solution. Results are presented in Fig. 7. A close-up on the last profiles is presented in Fig. 8. Note that the piston is initially located at $x = 1$ m and is moving towards $x = 0$ m. As expected the schemes give results very close to the analytical solutions, thus validating the ALE formulations. Fig. 8 shows that the Lax–Wendroff scheme behaves more like a low-pass filter than TTGC, underlining the higher precision of the latter.

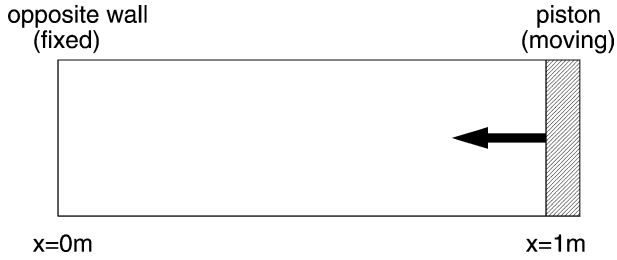

Fig. 6. Principle of the UAP test case.

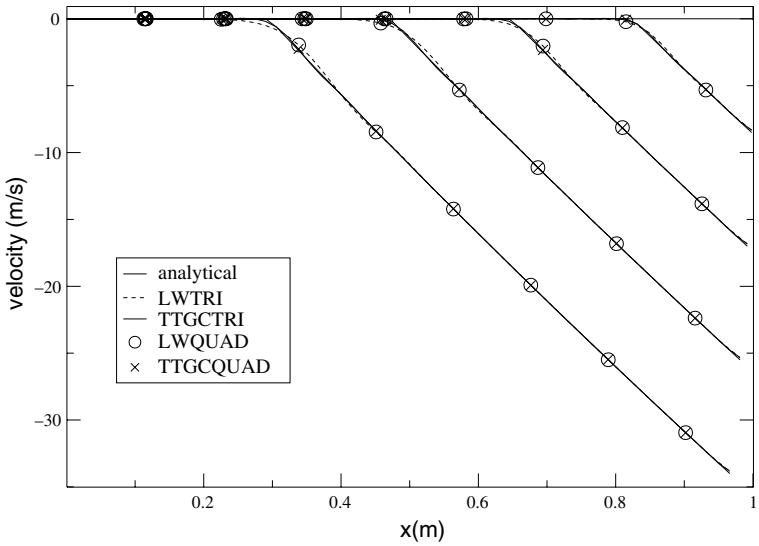

Fig. 7. Velocity profiles for the UAP test case at five successive instants.

8.5. Convergence order measurements

8.5.1. Error analysis for the Lax–Wendroff scheme

The Navier–Stokes equations can not be solved directly and must be discretized in space and time to find approximated solutions. Errors introduced by this discretization can be analysed and measured to estimate the quality of numerical schemes. Concerning the convective schemes, this kind of error analysis is usually done for the 1D advection equation for simplicity reasons:

$$\frac{\partial u}{\partial t} + a\frac{\partial u}{\partial x} = 0, \tag{82}$$

where a is a constant.

For the Lax–Wendroff scheme, the time discretization is obtained by a second-order Taylor development in time:

$$u_i^{n+1} = u_i^n + \Delta t\frac{\partial U}{\partial t} + \frac{\Delta t^2}{2}\frac{\partial^2 U}{\partial t^2} + \mathrm{O}[\Delta t^3]. \tag{83}$$

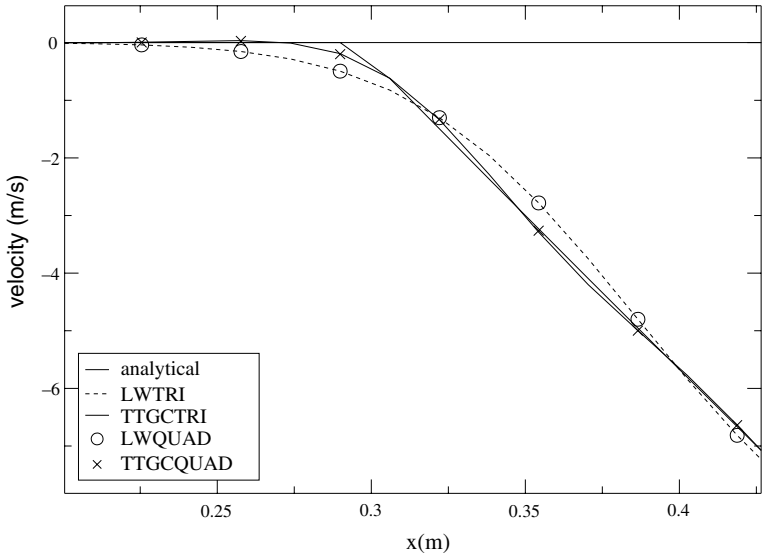

Fig. 8. Close-up on the last velocity profiles for the UAP test case.

Then temporal derivatives of Eq. (83) are replaced by spatial derivatives using Eq. (82):

$$u_i^{n+1} = u_i^n - \Delta t a \frac{\partial u}{\partial x} + \frac{\Delta t^2}{2} a^2 \frac{\partial^2 u}{\partial x^2} + \mathrm{O}[\Delta t^3]. \tag{84}$$

To remove the spatial derivatives of Eq. (84) two symmetric Taylor developments in space are needed:

$$u_{i+1}^n = u_i^n + \Delta x \frac{\partial u}{\partial x} + \frac{\Delta x^2}{2} \frac{\partial^2 u}{\partial x^2} + \mathrm{O}[\Delta x^3], \tag{85}$$

$$u_{i-1}^n = u_i^n - \Delta x \frac{\partial u}{\partial x} + \frac{\Delta x^2}{2} \frac{\partial^2 u}{\partial x^2} + \mathrm{O}[\Delta x^3]. \tag{86}$$

Finally, the *CFL* number defined as $CFL = a\Delta t/\Delta x$ is introduced to obtain the discrete Lax–Wendroff scheme:

$$u_i^{n+1} = u_i^n - \Delta t a \frac{u_{i+1}^n - u_{i-1}^n}{2\Delta x} + \frac{\Delta t^2}{2} a^2 \frac{u_{i+1}^n - 2u_i^n + u_{i-1}^n}{\Delta x^2} + \mathrm{O}[(\Delta t)^3] + \mathrm{O}[CFL\Delta x^3 + CFL^2\Delta x^3]. \tag{87}$$

A temporal and a spatial errors appear in Eq. (87). Since the Lax–Wendroff scheme is stable for *CFL* numbers less than one, it implies that the leading term of the spatial error is $\mathrm{O}[CFL\Delta x^3]$.

It is interesting to note that for a given simulation time, the spatial error is not influenced by the *CFL* value. This is not the case for the temporal error. If for a fixed *CFL* number, the simulation requires n time steps, the total spatial error is: $\mathrm{O}[n\ CFL\Delta x^3]$. Dividing the *CFL* by the ratio r, the mean time step is also divided by r and the number of iterations is multiplied by r. Finally, the total spatial error remains the same. This result is a property of centered schemes and can also been demonstrated for TTGC.

8.5.2. Spatial convergence order measurements

In compressible codes, both flow vortices and acoustic waves are convected. For each type of structure, a CFL can be defined:

$$CFL_{\text{conv}} = \frac{\Delta t\ u_{\max}}{\Delta x} \quad \text{and} \quad CFL_{\text{acou}} = \frac{\Delta t\ |u_{\max} + c|}{\Delta x} \tag{88}$$

and

$$CFL_{\text{conv}} = \frac{M}{1+M} CFL_{\text{acou}}, \tag{89}$$

where M is the Mach number. The stability condition of the numerical scheme is of the form:

$$\max(CFL_{\text{acou}}, CFL_{\text{conv}}) < CFL_{\max}. \tag{90}$$

For subsonic flows ($M < 0.3$), $M/(1 + M)$ is small and CFL_{conv} is far smaller than CFL_{acou}. The non-acoustic structures of the flow are thus well time-resolved and the numerical errors are mainly caused by the spatial resolution.

The purpose of the following test cases is to characterize the convective properties of the ALE schemes for the non-acoustic structures. CFL_{acou} is fixed at 0.7 and the influence of the spatial resolution on the convergence order is studied. Some additional tests about the influence of the CFL number are also presented to underline the fact that spatial errors prevail on temporal errors. The spatial error measurements are performed for two analytical solutions of the Euler equations. The first case is linear and consists in the convection of a Gaussian profile of a species k on periodic meshes. The flow velocity is uniform in order to obtain the same profile as the initial one after a convective time τ_{conv}. The principle of this linear case is illustrated in Fig. 9. The second test case is non-linear. It consists of a vortex convected by a uniform flow on a periodic mesh. After a convective time τ_{conv}, supposing that there are no interactions between the various vortices on the infinite domain, the vortex profile should be the same as the initial one. This test is illustrated in Fig. 10. For these two cases the numerical error introduced by the schemes

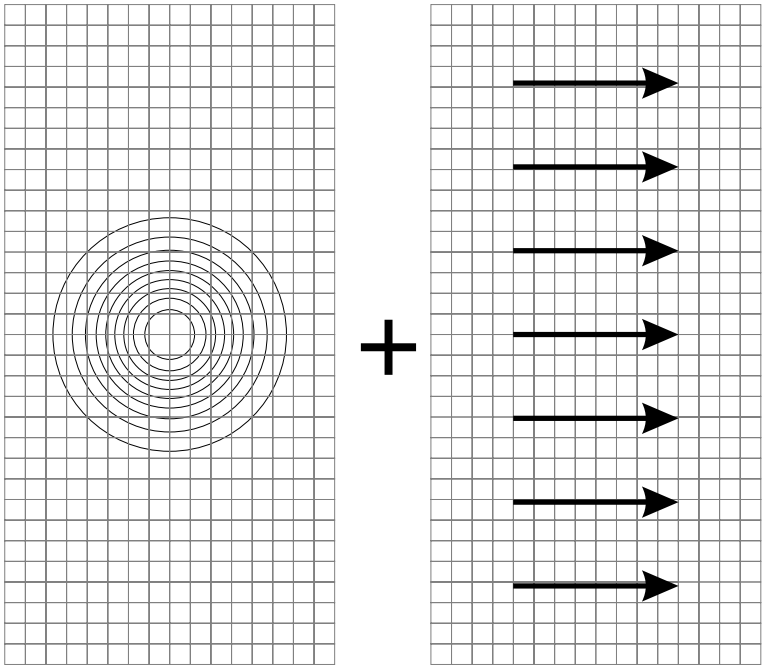

Fig. 9. Principle of the scalar convection case.

is estimated by the L2 norm of the difference between the initial profile and the profile at $t = \tau_{conv}$. The meshes are initially composed of regular quadrangles for which different resolutions are considered. The size of the different meshes are 21×41, 41×81 and 81×161 which correspond, respectively, to 13, 25 and 49 nodes in the Gaussian profile or in the vortex. To evaluate the influence of the ALE schemes on the convergence order the meshes undergo different deformation laws. The first law (see Fig. 11) consists of a sinusoidal 1D compression (1DC) which is orthogonal to the convective direction. The period of the deformation is denoted τ_u. The second law (see Fig. 12) is a sinusoidal radial contraction (RC) of period τ_c. The combination of these two laws provides four cases that are defined and described in Table 2. For cases A and B the elements remain regular during the simulation, while they do not for cases C and D. Fig. 13 and Fig. 14 show the numerical error as a function of the initial element size for the linear and the non-linear cases. For the FV Lax–Wendroff scheme, the precision is independent of the mesh movement with a convergence order close to the theoretical value of 2. For TTGC, the results depend on the regularity of the mesh. The numerical errors for cases A and B are nearly identical and the convergence order is close to the order measured by Colin and Rudgyard [15] on regular bilinear elements, i.e. between 3 and 4. For cases C and D the order corresponds to the order measured by Colin and Rudgyard [15] on perturbed bilinear meshes, i.e. between 2 and 3. It should be underlined that even on perturbed meshes, the accuracy of TTGC is far better than the Lax–Wendroff scheme.

To verify that spatial errors prevail on temporal errors for similar cases and particularly turbulent cases, the previous tests have been rerun with different *CFL* numbers. Table 3 gives an example of results for the 21×41 Gaussian convection case on fixed grid. For very different *CFL* numbers, the measured error remains equal to its reference value. It implies that the measured error is mainly due to spatial discretization errors as demonstrated in Section 8.5.1 for subsonic compressible flows.

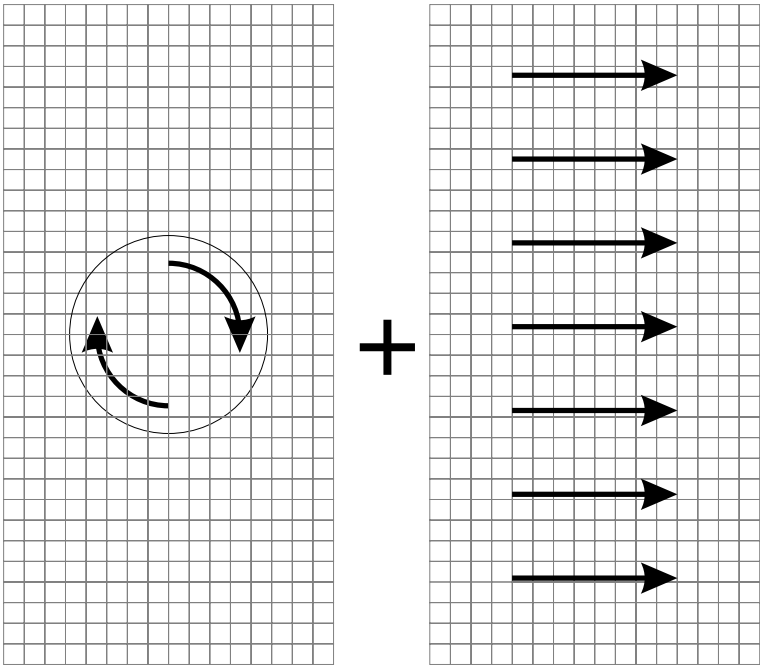

Fig. 10. Principle of the vortex convection case.

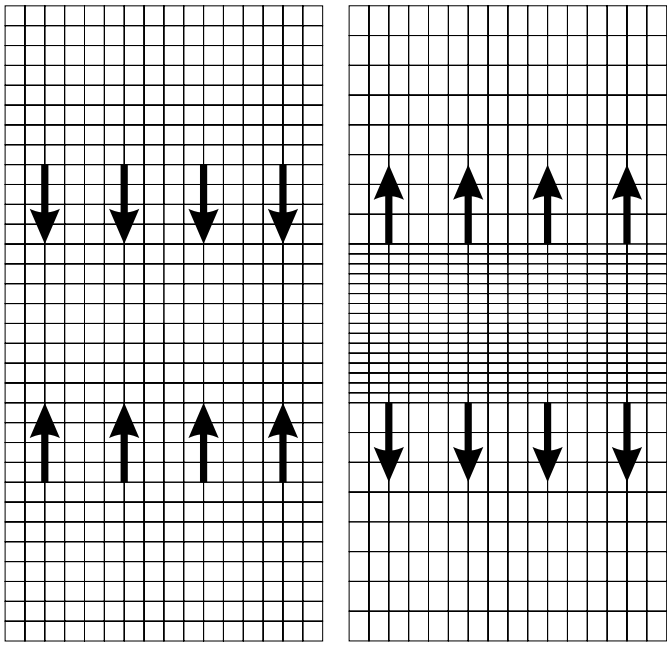

Fig. 11. 1D compression–expansion mesh deformation.

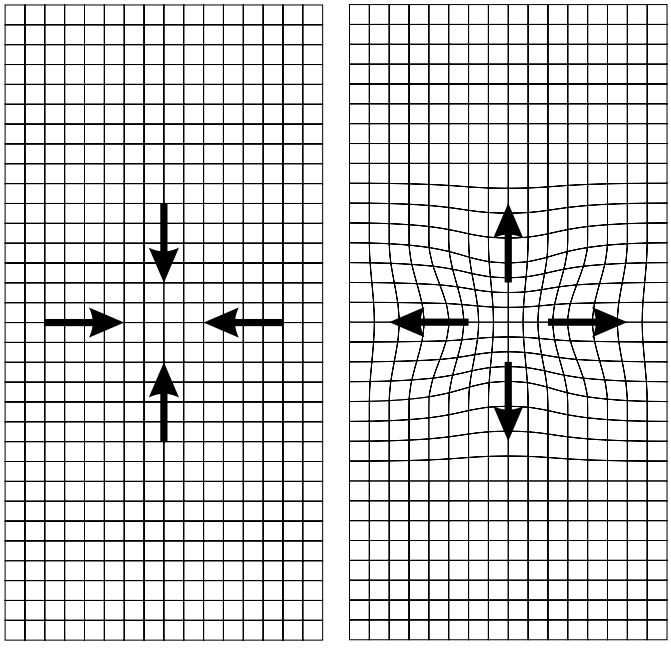

Fig. 12. Radial contraction–expansion mesh deformation.

Table 2
Mesh movement cases

Case	Type	Parameters	$\lvert\dot{X}\rvert_{\max}$
A	Fixed		
B	1DC	$\frac{\tau_u}{\tau_{\text{conv}}} = 0.2$	26.2 m/s
C	1DC + RC	$\frac{\tau_u}{\tau_{\text{conv}}} = \frac{\tau_c}{\tau_{\text{conv}}} = 0.2$	26.2 m/s
C	1DC + RC	$\frac{\tau_u}{\tau_{\text{conv}}} = 0.2,\ \frac{\tau_c}{\tau_{\text{conv}}} = 0.125$	27.8 m/s

1DC: mono-dimensional compression; RC: radial compression.

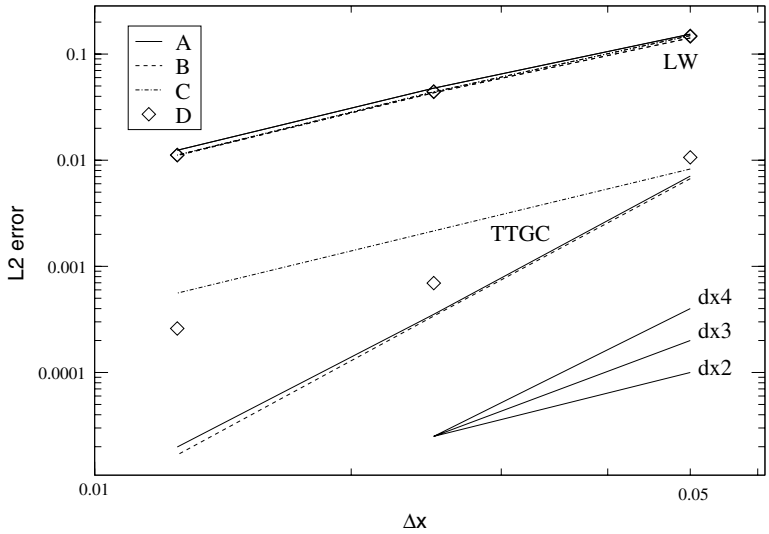

Fig. 13. Error for the scalar convection case versus mesh size.

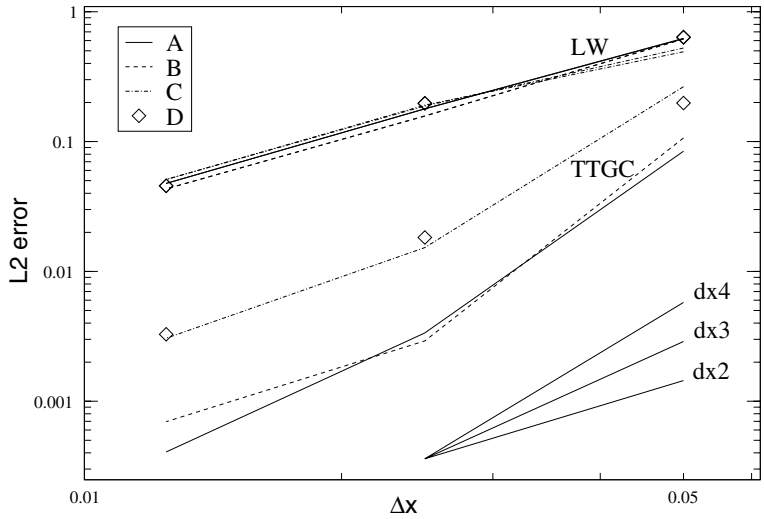

Fig. 14. Error for the vortex convection case versus mesh size.

Table 3
Error for the 21×41 Gaussian convection case versus *CFL* value

CFL	L2 error
0.7	0.1535
0.1	0.1541
0.01	0.1543

9. Conclusions

A methodology for unsteady multispecies reacting flows on fixed and moving grids has been presented and tested in simple laminar flows (applications to DNS and LES of fully turbulent cases may be found in [16,52] or [54]). The importance of boundary conditions was stressed and a new simple formulation to implement characteristic boundary conditions in compressible DNS/LES codes was described. This formulation has been tested and results for laminar flames are presented. It was also shown that high-order (second and third order) schemes can be constructed on hybrid moving grids but that their derivation required some care to preserve accuracy. These schemes have been tested on various cases such as uniform flow on moving grids, uniformly accelerated pistons, scalar convection and vortex propagation on deforming grids, to confirm the validity of the various methods and measure the exact order or precision of these techniques. The mesh deformations used in these cases are representative of the distortions that can be found in many practical configurations such as piston engines. But when the grid becomes too distorted during a simulation, the ALE method can be used in conjunction with interpolation techniques to change mesh and keep numerical dissipation low.

References

[1] T. Poinsot, D. Veynante, in: R.T. Edwards (Ed.), Theoretical and Numerical Combustion, 2001.
[2] N. Peters, Turbulent combustion, Cambridge University Press, Cambridge, 2000.
[3] C. Angelberger, D. Veynante, F. Egolfopoulos, Large Eddy Simulations of chemical and acoustic forcing of a premixed dump combustor, Flow Turbul. Combust. 65 (2) (2000) 205–222.
[4] H. Pitsch, H. Steiner, Large Eddy Simulation of a turbulent piloted methane/air diffusion flame (Sandia flame D), Phys. Fluids 12 (2000) 2541–2554.
[5] H. Pitsch, L.D. de la Geneste, Large Eddy Simulation of premixed turbulent combustion using a level-set approach, in: Proc. of the Comb. Institute, vol. 29, 2002, pp. 2001–2008.
[6] D. Caraeni, C. Bergström, L. Fuchs, Modeling of liquid fuel injection evaporation and mixing in a gas turbine burner using Large Eddy Simulations, Flow Turbul. Combust. 65 (2000) 223–244.
[7] K. Mahesh, G. Constantinescu, P. Moin, A numerical method for Large-Eddy Simulation in complex geometries, J. Comput. Phys. 197 (2004) 215–240.
[8] M.M. Rai, P. Moin, Direct simulations of turbulent flow using finite-difference schemes, J. Comput. Phys. 96 (1991) 15–53.
[9] S.I. Möller, E. Lundgren, C. Fureby, Large Eddy Simulations of unsteady combustion, in: 26th Symp. (Int.) on Comb., The Combustion Institute, Pittsburgh, 1996, pp. 241–248.
[10] W.W. Kim, S. Menon, An unsteady incompressible navier stokes solver for LES of turbulent flows, Int. J. Numer. Meth. Fluids 31 (1999) 983–1017.
[11] N. Branley, W.P. Jones, Large Eddy Simulation of a turbulent non-premixed flame, Combust. Flame 127 (2001) 1914–1934.
[12] C.D. Pierce, P. Moin, Progress-variable approach for Large Eddy Simulation of non-premixed turbulent combustion, J. Fluid Mech. 504 (2004) 73–97.
[13] P.E. DesJardin, S.H. Frankel, Large Eddy Simulation of a nonpremixed reacting jet: application and assessment of subgrid-scale combustion models, Phys. Fluids 10 (1998) 2298–2314.
[14] J. Schlüter, T. Schönfeld, LES of jets in cross flow and its application to gas turbine burners, Flow Turbul. Combust. 65 (2000) 177–203.

[15] O. Colin, M. Rudgyard, Development of high-order Taylor–Galerkin schemes for unsteady calculations, J. Comput. Phys. 162 (2) (2000) 338–371.
[16] A. Kaufmann, F. Nicoud, T. Poinsot, Flow forcing techniques for numerical simulation of combustion instabilities, Combust. Flame 131 (4) (2002) 371–385.
[17] K.W. Thompson, Time dependent boudary conditions for hyperbolic systems, J. Comput. Phys. 68 (1987) 1–24.
[18] C. Hirsch, Numerical Computation of Internal and External Flows, Wiley, New York, 1988.
[19] M. Giles, Non-reflecting boundary conditions for Euler equation calculations, AIAA J. 28 (1990) 2050–2058.
[20] M. Baum, T. Poinsot, D. Thévenin, Accurate boundary conditions for multicomponent reactive flows, J. Comput. Phys. 116 (1994) 247–261.
[21] N. Okong'o, J. Bellan, Consistent boundary conditions for multicompoment real gas mixtures based on characteristic waves, J. Comput. Phys. 176 (2002) 330–344.
[22] W.T. Ashurst, N. Peters, M.D. Smooke, Numerical simulation of turbulent flame structure with non-unity Lewis number, Combust. Sci. Technol. 53 (1987) 339–375.
[23] R.J. Cattolica, P.K. Barr, N.N. Mansour, Propagation of a premixed flame in a divided-chamber combustor, Combust. Flame 77 (1989) 101–121.
[24] P.K. Yeung, S.S. Girimaji, S.B. Pope, Straining and scalar dissipation on material surfaces in turbulence: implications for flamelets, Combust. Flame 79 (1990) 340–365.
[25] C.J. Rutland, A. Trouvé, Direct simulations of premixed turbulent flames with nonunity Lewis number, Combust. Flame 94 (1993) 41–57.
[26] D. Haworth, T. Poinsot, Numerical simulations of Lewis number effects in turbulent premixed flames, J. Fluid Mech. 244 (1992) 405–436.
[27] C.J. Rutland, J. Ferziger, Simulation of flame–vortex interactions, Combust. Flame 84 (1991) 343–360.
[28] C. Westbrook, F. Dryer, Simplified reaction mechanism for the oxidation of hydrocarbon fuels in flames, Combust. Sci. Technol. 27 (1981) 31–43.
[29] W.P. Jones, R.P. Lindstedt, Global reaction schemes for hydrocarbon combustion, Combust. Flame 73 (1988) 222–233.
[30] S. Zhang, C. Rutland, Premixed flame effects on turbulence and pressure related terms, Combust. Flame 102 (1995) 447–461.
[31] D. Veynante, T. Poinsot, Effects of pressure gradients on turbulent premixed flames, J. Fluid Mech. 353 (1997) 83–114.
[32] D. Veynante, A. Trouvé, K.N.C. Bray, T. Mantel, Gradient and counter-gradient scalar transport in turbulent premixed flames, J. Fluid Mech. 332 (1997) 263–293.
[33] B. Bédat, F. Egolfopoulos, T. Poinsot, Direct numerical simulation of heat release and nox formation in turbulent non premixed flames, Combust. Flame 119 (1) (1999) 69–83.
[34] M. Baum, D. Haworth, T. Poinsot, N. Darabiha, Direct numerical simulation H2/O2/N2 flames with complex chemistry in two-dimensional turbulent flows, J. Fluid Mech. 281 (1994) 1–32.
[35] G. Patnaik, K. Kailasanath, A computational study of local quenching in flame vortex interactions with radiative losses, in: 27th Symp. (Int.) on Combust., The Combustion Institute, Pittsburgh, 1998, pp. 711–717.
[36] M.Y.N. Tanahashi, M.T.M. Fujimura, Fine scale structure of H2-air turbulent premixed flames, in: S. Banerjee, J. Eaton (Eds.), 1st International Symposium on Turbulence and Shear Flow, 1999, pp. 59–64.
[37] D.R. Stull, H. Prophet, JANAF Thermochemical Tables, second ed., Report No. NSRDS-NBS 37, US National Bureau of Standards, 1971.
[38] J.O. Hirschfelder, C.F. Curtiss, R.B. Byrd, Molecular Theory of Gases and Liquids, Wiley, New York, 1969.
[39] A. Ern, V. Giovangigli, Multicomponent Transport Algorithms, Springer, Heidelberg, 1994.
[40] V. Giovangigli, Multicomponent Flow Modeling, Birkhäuser, Boston, 1999.
[41] F.A. Williams, Combustion Theory, Benjamin Cummings, Menlo Park, CA, 1985.
[42] J.C. Strikwerda, Initial boundary value problem for incompletely parabolic systems, Commun. Pure Appl. Math. 30 (1977) 797.
[43] T. Poinsot, S. Lele, Boundary conditions for direct simulations of compressible viscous flows, J. Comput. Phys. 101 (1) (1992) 104–129.
[44] T. Colonius, S. Lele, P. Moin, Boundary conditions for direct computation of aerodynamic sound generation, AIAA J. 31 (9) (1993) 1574–1582.
[45] T. Colonius, Numerically nonreflecting boundary and interface conditions for compressible flow and aeroacoustic computations, AIAA J. 35 (7) (1997) 1126–1133.
[46] K. Rowley, T. Colonius, Discretely nonreflecting boundary conditions for linear hyperbolic systems, J. Comput. Phys. 157 (2) (2000) 500–538.
[47] R. Verzicco, J. Mohd-Yusof, P. Orlandi, D. Haworth, Large-Eddy Simulation in complex geometric configurations using boundary body forces, AIAA J. 38 (2000) 427–433.
[48] C. Hirt, A. Amsden, J. Cook, An Arbitrary Lagrangian–Eulerian computing method for all flow speeds, J. Comput. Phys. 14 (1974) 227–253.

[49] A. Masud, T. Hughes, A space–time Galerkin/least-squares finite element formulation of the Navier–Stokes equations for moving domain problems, Comput. Meth. Appl. Mech. Eng. 146 (1997) 91–126.
[50] T. Tezduyar, M. Behr, J. Liou, A new strategy for finite element computations involving moving boundaries and interfaces – the deforming-spatial-domain/space–time procedure: I. the concept and the preliminary tests, Comput. Meth. Appl. Mech. Eng. 94 (1992) 339–351.
[51] C. Farhat, P. Geuzaine, C. Grandmont, The discrete geometric conservation law and the nonlinear stability of the ale schemes for the solution of flow problems on moving grids, J. Comput. Phys. 174 (2) (2001) 669–694.
[52] L. Selle, G. Lartigue, T. Poinsot, R. Koch, K.-U. Schildmacher, W. Krebs, B. Prade, P. Kaufmann, D. Veynante, Compressible Large-Eddy Simulation of turbulent combustion in complex geometry on unstructured meshes, Combust. Flame 137 (4) (2004) 489–505.
[53] L. Landau, E. Lifchitz, Physique Theorique – Tome 6: Mecanique des Fluides, Librairie du Globe, Editions MIR, 1984.
[54] C. Prière, L. Gicquel, A. Kaufmann, W. Krebs, T. Poinsot, LES of mixing enhancement: LES predictions of mixing enhancement for jets in cross-flows, J. Turbul. 5 (1) (2004) 005.